Transition Galaxies: The Evolution of Environmental Quenching

by

Karen McNab

A thesis
presented to the University of Waterloo
in fulfillment of the
thesis requirement for the degree of
Master of Science
in
Physics

Waterloo, Ontario, Canada, 2021

Author's Declaration

This thesis consists of material all of which I authored or co-authored: see Statement of Contributions included in the thesis. This is a true copy of the thesis, including any required final revisions, as accepted by my examiners.

I understand that my thesis may be made electronically available to the public.

Statement of Contributions

This research was conducted under the supervision of Michael Balogh, with contributions and consultations from the GOGREEN collaborators, including Greg Rudnick, Adam Muzzin, Remco van der Burg, Benedetta Vulcani, Kristi Webb and Anya Forestell. The analysis in this work is based on catalogues produced by the GOGREEN collaborators (http://gogreensurvey.ca). Michael Balogh provided the conceptualization of the project as a whole, and the framework for determining the transition timescales included in Section 3.3. Figure 3.3 was generated by Michael Balogh, and Figure 4.6 was generated by Kristi Webb. Figure 1.1 was pulled from Behroozi et al. (2019). All other work in this thesis is my own.

Abstract

We study the evolution of environmental quenching using a photometric selection of transition galaxies in GOGREEN- which encompasses clusters between 1<z<1.5 spanning a range in halo mass from $10^{13} \leq \log(M/M_{\odot}) \leq 10^{15}$. We split the galaxies in GOGREEN into three populations using their NUV-V, V-J colours and define a green valley between the quiescent and star-forming populations, making use of the deep B, g, and V band imaging from the survey. The green valley makes up $\sim 10\%$ of the cluster population, and shows no strong dependence on cluster-centric radius, and also show a similar abundance to the field volume outside 1 Mpc. We find that the stellar mass function of the green valley is intermediate to the quiescent and star-forming SMFs, and that their shape more resembles the quiescent stellar mass function, specifically in the flat, faint-end slope. Using the stellar mass functions of each population, we build a simple framework where we determine the different parameters associated with the transitioning population. We assume that a fraction $\beta(t)$ of the star-forming population quenches every Gyr, as a result of environment, and that they spend a time τ in the green valley as this happens. We find that the rate at which galaxies are entering the quiescent population as a result of environmental quenching (β) is consistent with the past average rate (β_{avg}) at 0.08, and that the galaxies entering the green valley stay there for a time $\tau < 1$ Gyr, which is expected from rapid environmental quenching mechanisms in clusters. We find an excess of spectroscopic post-starbursts and blue-quiescent galaxies in the cluster indicate that much of this transition is happening via fast-quenching. The environmental processes responsible for quenching the star-formation in cluster galaxies appears to already be underway, even at the early epochs considered here.

Dedication

This work is dedicated to Leia, Lucas and Aurora. I cannot wait to see all that you accomplish in the future.

Table of Contents

List of Figures

List of Tables

Chapter 1

Introduction

In a ΛCDM Universe, gravitational collapse drives the growth of dark matter haloes. The growth of haloes happens hierarchically where low mass haloes are formed earlier and are built up via accretion and mergers (White & Frenk, 1991). This is evident when looking at the two-point correlation function, which characterizes the spatial distribution or clustering of galaxies. This shows that the clustering of galaxies is much stronger on small scales and weaker on larger scales, where we see good agreement with what is predicted with cold dark matter models (Peacock et al., 2001; Cole et al., 2005). As dark matter haloes evolve, the baryonic gas in them settles into the potential wells of the haloes and begins to form galaxies. This requires a variety of processes including gas cooling, star-formation and feedback processes (White & Frenk, 1991).

Dark matter haloes contain gas in a variety of phases, and therefore undergo cooling via multiple processes, including Bremmstrahlung emission, recombination, excitation and de-excitation. Since these cooling methods depend on the proximity of the particles involved, cooling is more effective in dense regions, but all result in the baryonic matter separating from the dark matter forming a proto-galaxy in the center of the halo. The gas in the dark matter halo will eventually cool and flow inward and collapse under its own gravity, resulting in the formation of stars. However, we only see a small portion of baryons in cold gas or stars (Cole, 1991), which is contrary to the above point. This requires some mechanism that either re-heats the gas, or prevents it from cooling in the first place. There are feedback processes that may contribute to this, including that from supernovae and active galactic nuclei (AGN). Both of these objects produce vast amounts of energy capable of heating the gas surrounding them, and throughout the galaxy.

Taking a look at the stellar-halo-mass relation shows where these feedback mechanisms
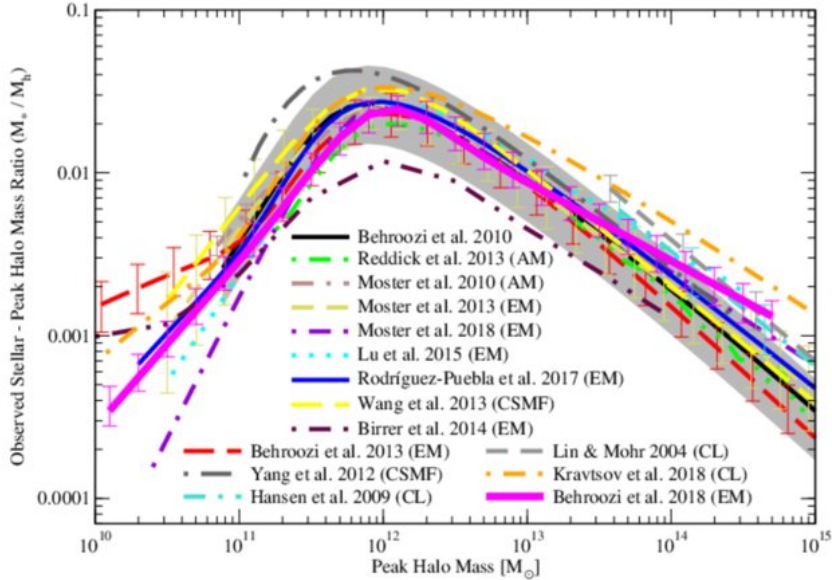
Figure 1.1: A figure from Behroozi et al. (2019), showing the stellar-halo mass relation determined by a variety of techniques. A clear peak is present in all cases, where the slope of the relation is suppressed on the left by feedback from supernovae and on the right by AGN feedback.

are the most effective. At low redshift, galaxies in a halo of given mass are more massive than those at high redshift in a halo of the same mass, shown in Figure 1.1 from Behroozi et al. (2019). Since dark matter haloes grow over time, this indicates that the haloes accrete dark matter faster than galaxies increase their stellar mass. There is a characteristic peak in the stellar-halo-mass relation, with a decline on either side, indicating the regions where the feedback mechanisms are most prevalent– feedback from supernovae is more effective at reheating and expelling gas in lower mass haloes where the gravitational well is shallow, and AGN feedback is more effective at the high mass end where black holes are more massive (Moster et al., 2010).

When looking at the total stellar mass function of galaxies, we can see that massive galaxies were in place at higher redshift, with low-mass ones being built up over time (Muzzin et al., 2013a; McLeod et al., 2021). When comparing the stellar mass function (SMF) of baryonic matter to that of the CDM halo mass function, there are clear discrepancies (Bower et al., 2006). This anti-hierarchical growth, and distinction in the shape of the SMFs makes it clear that galaxy evolution does not simply trace the dark matter.

2

The star-formation rate of star-forming galaxies is nearly proportional to stellar mass, at all redshifts to at least $z = 2.5$ (Salim et al., 2007; Noeske et al., 2007; Patel et al., 2009; Whitaker et al., 2012), yet the SMF of these galaxies evolves only modestly with time (Muzzin et al., 2013b). In contrast, the abundance of non-starforming (passive, or quiescent) galaxies builds up rapidly with time. This indicates that there is a transition – quenching – of the galaxies from the blue star-forming sequence to the red as they stop forming stars (Faber et al., 2007). The bimodality in the star-formaion rate and colour distributions of galaxies implies that this transition must be fairly rapid (Wetzel et al., 2012). The transition rate into quiescence is also primarily dependent on stellar mass, where galaxies with high masses are more likely to be quenched (Takamiya et al., 1995; Strateva et al., 2001; Muzzin et al., 2013a). Studying the intermediate region between the star-forming and quiescent phases of galaxy growth can provide constraints on the nature of galaxy transformation and the rate at which galaxies undergo them, and comparing transition galaxies in the cluster with those in the field can help constrain environmental impacts on galaxy evolution.

Such transition galaxies have often been used to trace the quenching rate over time and as a function of stellar mass (Socolovsky et al., 2018; Tran et al., 2004; Pattarakijwanich et al., 2016; Wild et al., 2016, 2020). The slow, undisturbed fading of star-formation in galaxies can account for most of the quiescent population, though the excess of some transition galaxies near the edges of clusters indicates a more rapid quenching process in addition to this underlying fading, leaving two quenching pathways in galaxy evolution. The redshift evolution of the fraction of transition galaxies remains relatively unconstrained. This is in part due to differing definitions used to select transitioning galaxies, and with which assumed parent population they are compared to. (Belli et al., 2019; Carnall et al., 2019).

We have long known that galaxy properties depend on environment, starting with the observations of the environmental dependence of galaxy morphology. In higher density, cluster environments the galaxy population is dominated by early-type S0 and ellipticals, while in lower density field environments we see more late-type spirals. This implies that galaxy evolution depends on the environment in which a galaxy resides, where star-formation is suppressed when a galaxy enters the high density region of a cluster (Dressler, 1980). Many other galaxy properties have shown similar environmental dependencies, specifically that galaxies in clusters are redder, more massive, more concentrated, have lower gas fractions and lower specific star-formation rates than their field counterparts (Kauffmann et al., 2004; Baldry et al., 2006; Weinmann et al., 2006). However, since these galaxy properties are all correlated with each other, it is unclear which fundamentally display an environmental dependence.

At fixed stellar mass, galaxies in dense environments are more likely to be quiescent,

at all redshifts $z \lesssim 2$ (Balogh et al., 2016), than their field counterparts. Using galaxy colours and the slope of the red-sequence can help constrain the star-formation histories, and show that cluster galaxies formed their stars at early times, and evolve passively from that point. However, the fraction of quiescent galaxies also depends on their environment (Lewis et al., 2002; Gómez et al., 2003; Baldry et al., 2006). Empirically, the additional environmental quenching is separable from stellar mass dependence (Baldry et al., 2006; Peng et al., 2010). This suggests that additional environmental quenching processes are contributing to the build up of the red sequence in clusters.

Different mechanisms have been proposed in order to explain the differences between the cluster and field populations. In order for quenching to happen, there needs to be some removal of the cold gas reservoir, and since internal quenching mechanisms cannot alone account for the amount of quenching we see in clusters, some environmental effects must be occurring. Possibilities include tidal disruption, ram pressure stripping (Gunn & Gott III, 1972), strangulation Cole et al. (2000), and harassment (Moore et al., 1996). Ram-pressure stripping causes the gas of a galaxy to be stripped away due to the galaxy moving through the cluster or similarly, tidal disruptions and other gravitational interactions between galaxies can remove the cold gas needed for star-formation. Current simulations and observations show that a combination of these effects is likely contributing to the quenching of galaxies, where ram-pressure stripping is dominant in inner cluster regions of high density, and that gravitational mechanisms play more of a role in the lower density regions.

Our focus here is on this environmental component of galaxy evolution, where there is a large body of literature on the use of transition galaxies to trace quenching in dense environments (Zabludoff et al., 1996; Balogh et al., 1999; Poggianti et al., 1999, 2009; Paccagnella et al., 2019; Hogg et al., 2006; Yan et al., 2009; Mok et al., 2013, 2014). This work was pioneered with the identification of "E+A" galaxies in clusters (Dressler & Gunn, 1983, 1992; Couch & Sharples, 1987). These galaxies show strong Balmer absorption lines, indicative of recent star formation, but no signs of ongoing star-formation since they lack [OII] or Hα emission.

The identification of such galaxies requires spectroscopy, and is most sensitive to quenching that occurs rapidly following a burst of star formation Couch & Sharples (1987). An alternative approach has been to use the "green valley" in photometric data. Originally the green valley was defined as the region between the red and blue sequences in a colour-magnitude or colour-stellar mass diagram (Schiminovich et al., 2007; Schawinski et al., 2014; Vulcani et al., 2015). However, this definition includes many dusty star-forming galaxies, especially at high masses and high redshifts. This is mitigated by using two colour diagrams like (U-V) vs (V-J), and again identifying the green valley as the region between

the quiescent and star forming populations (Mendez et al., 2011; Mok et al., 2013, 2014). Further, the use of the rest-frame near-ultraviolet (NUV) colour, can provide a greater separation between the star-forming and quiescent population and thus greater sensitivity to any transitioning galaxies (Moutard et al., 2016, 2018; Salim et al., 2007). Others have used different combinations of colours (Wild et al., 2016; Leja et al., 2019), star-formation rates (Salim, 2014; Schiminovich et al., 2007) or spectral types (Suess et al., 2020) in order to identify transitioning galaxies.

The Gemini Observations of Galaxies in Rich Early ENvironments (GOGREEN) survey consists of spectroscopy and deep, multi-wavelength photometry of galaxies in dense cluster environments at $1 < z < 1.5$, spanning a large range in halo mass, selected to be representative of progenitors of today's clusters. In previous work we have studied the star formation histories (Old et al., 2020; Webb et al., 2020) and stellar mass functions (Chan et al., 2019; van der Burg et al., 2020) of the galaxies in these clusters. A general picture is emerging in which environmental quenching plays a significant role in galaxy evolution even at these redshifts. However, the nature of that quenching appears to be quite different from what dominates clusters at lower redshift (Balogh et al., 2016). In particular, van der Burg et al. (2020) suggest that most of the quiescent galaxies in these clusters may have already been in place at much earlier times, rather than transformed following accretion onto an established cluster (see also Poggianti et al., 2006).

In this paper we make use of deep rest frame-NUV photometry of GOGREEN galaxies to select the intermediate green valley in colour-colour space. This approach is taken to capture *all* galaxies as the pass from the star-forming to quiescent sequence, independent of the quenching mechanism. It therefore provides a complete census of the transition rate, though it is not "pure" since it will also include substantial contamination from edge-on spiral galaxies and galaxies with slowly declining star formation rates (Schawinski et al., 2014). This makes it complementary to other studies that select populations that are more pure, but sensitive to particular quenching pathways (Poggianti et al., 2006; Muzzin et al., 2013a; Belli et al., 2019; Carnall et al., 2019).

Studying this population in both the cluster and the field at high redshift can allow us to determine if there is environmental dependencies on the processes that quench these galaxies, and utilizing a deep photometric sample enables us to look at relatively low stellar masses, shown in Table 2.1.

Chapter 2

Data

2.1 The GOGREEN Survey

The GOGREEN project is a spectroscopic and photometric survey of 21 galaxy clusters and groups at $1 < z < 1.5$. For each system, deep ($\gtrsim 24$ AB) imaging is available in ~ 11 bands between u and 4.5μm. The survey is built upon a large multiobject spectroscopy campaign with Gemini GMOS, targeting faint ($z' < 24.5$ and $[3.6\mu m] < 22.5$) galaxies over a $5.5\,'$ field around each system. The spectroscopic sampling is unbiased with respect to galaxy type for $M \gtrsim 2 \times 10^{10} M_\odot$, and secure redshifts are available for over 2200 galaxies. More details on the survey strategy and data are available in Balogh et al. (2017) and Balogh et al. (2021).

This work will focus on the eleven massive clusters[1] in the GOGREEN sample at $z < 1.4$, selected from the SpARCS Wilson et al. (2009); Muzzin et al. (2009); Demarco et al. (2010) and SPT Brodwin et al. (2010); Foley et al. (2011); Stalder et al. (2013) surveys. With one exception (SpARCS1034+5818), these systems have velocity dispersions of $500 < \sigma/\text{km/s} \lesssim 900$, corresponding to halo masses $10^{14} \lesssim M/M_\odot \lesssim 10^{15}$ Balogh et al. (2021). We assume a Chabrier initial mass function and a flat ΛCDM cosmological model. The relevant cluster-specific parameters are included in Table 2.1.

---

[1] At the time of writing, K-band imaging observations were not complete for the final cluster, SpARCS1033+5753.

6

Table 2.1: Relevant properties of the eleven GOGREEN clusters analysed in this work. These include the mean redshift (column 2), virial radius R_{200} (column 2), centre (identified as the location of the most massive galaxy) (column 3), and the stellar mass limit of the photometric catalogues (column 4).

Cluster	Redshift	R_{200} (Mpc)	RA, Dec (J2000)	$log(M_{*,lim})$ ($M_\odot$)
SPTCL-0205	1.320	0.755	02:05:48.19, -58:28:49.0	9.90
SPTCL-0546	1.067	1.174	05:46:33.67, -53:45:40.6	9.64
SPTCL-2106	1.131	1.226	21:06:04.59, -58:44:27.9	9.79
SpARCS-0035	1.335	0.929	00:35:49.68, -43:12:23.8	9.70
SpARCS-0219	1.325	0.791	02:19:43.56, -05:31:29.6	9.90
SpARCS-0335	1.368	0.672	03:35:03.56, -29:28:55.8	10.07
SpARCS-1034	1.385	0.237	10:34:49.47, +58:18:33.1	9.55
SpARCS-1051	1.035	0.875	10:51:11.23, +58:18:02.7	9.35
SpARCS-1616	1.156	0.918	16:16:41.32, +55:45:12.4	9.59
SpARCS-1634	1.177	0.845	16:34:37.00, +40:21:49.3	9.50
SpARCS-1638	1.196	0.705	16:38:51.64, +40:38:42.9	9.54

2.2 Galaxy Selection

For this project we primarily use the photometric sample of galaxies, for which photometric redshifts and rest frame colours have been obtained as described in van der Burg et al. (2020) and Balogh et al. (2021). van der Burg et al. (2020) determine mass limits for the clusters based on the depth of the k-band photometry, finding that they range from $9.5 \leq \log(M/M_\odot) \leq 10.1$. For the purpose of this thesis our sample is limited to galaxies with $\log(M/M_\odot) \geq 9.5$, with good quality photometry in the K-band (SExtractor flags < 4) and within the redshift range $1 < z < 1.5$. We remove stars based on the SExtractor star parameter (< 0.96)[2].

Galaxies were classified as "star-forming" (SF), "quiescent" (Qui) or "green-valley" (GV), based on their positions in rest-frame (NUV-V) and (V-J) colour space (Schawinski et al., 2014; Smethurst et al., 2015; Moutard et al., 2018, hereafter referred to as NUV-V-J,), as shown in Figure 2.1. The green valley was selected by-eye to encompass the region between the two over-densities of the quiescent and star-forming population in NUV-V-J space, and was chosen to span the entirety of the colour-colour space as to ensure that any

---

[2]This approach to star-galaxy separation is different from the colour-based criterion used in van der Burg et al. (2020) and Balogh et al. (2021).

galaxy transitioning from star-forming to quiescence *must* pass through it, regardless of the evolutionary path they take. Use of the NUV colour on the y-axis provides more than five magnitudes of dynamic range between the bluest and reddest galaxies. We show our population selections in colour-colour space in Table 2.2. This makes it a more promising diagnostic to identify intermediate, or transition, populations in comparison to the more commonly used UVJ diagram (Williams et al., 2009; Muzzin et al., 2013b; van der Burg et al., 2013). The use of this diagnostic is made possible by the very deep $V-$ (> 25.3) and $g-$ (> 26) band imaging of GOGREEN clusters (van der Burg et al., 2020), so that most galaxies above our mass limit are directly detected at wavelengths close to the rest-frame NUV. We demonstrate this explicitly in Figure 2.2, where we show the fraction of each galaxy type that is detected at $> 3\sigma$ in either the $g-$ band (northern clusters, with Subaru Suprimecam imaging) or $V-$ band (southern clusters, from VLT-VIMOS), as a function of stellar mass. For $M > 10^{10.5}M_\odot$, most star-forming and green valley galaxies have detections in these filters, which correspond closely to the rest-frame NUV. Even at the lowest stellar masses we probe, about a third of the green valley galaxies are detected. Non-detections could, in principle, be redder in (NUV-V) than predicted, though this colour is still constrained by the SED fit to the redder filters. Therefore, some green valley galaxies could have intrinsic colours more typical of the quiescent population, and have been scattered blue-ward due to photometric uncertainties. We will address this caveat where relevant in the context of our results, but it does not have a qualitative effect on our conclusions.

The slope of the green valley region was chosen to match that of the star-forming sequence, and the width was chosen to be a balance between making the region small enough to reduce contamination from the other populations, and making it too narrow-causing an underestimate of the green valley. The potential contamination from the other populations due to uncertainties in our NUV-V colour would cause the green valley to be populated with quiescent galaxies, however if this contamination were significant, we would expect to see the green valley replicate the radial distribution of the quiescent population (Figure 3.1). Since we do not see this same radial dependence in the green valley, we have determined that the contamination is not significant enough to impact the results in this paper.

Candidate cluster members are selected using a photometric redshift (±0.16) and radius (< 1 Mpc) cut around the cluster centre. The field sample is selected from all galaxies with photometric redshifts $1 < z < 1.5$ and at $r > 1$ Mpc from the centre of each cluster. This may not be representative of a random field sample, and could include galaxies associated with the cluster and surrounding structures. However, we show in Section 3.2 that the stellar mass functions of different galaxy types in our field sample are similar to those of

8
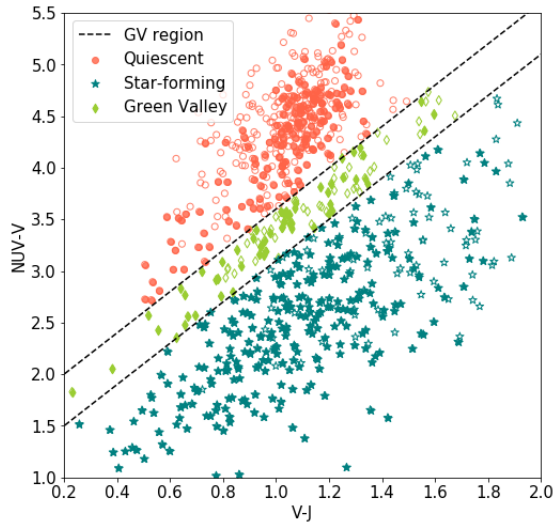
Figure 2.1: We define the quiescent, star-forming and green valley populations in (NUV-V) (V-J) colour space. The quiescent galaxies (red) are defined as any galaxies lying above the top line, with the star forming (blue) region below the bottom line. The green valley (green) galaxies are those in the region in between the lines, chosen to coincide with the relatively low density region between the other two populations. This is a zoomed in region in colour-colour space, with 1.8% of the sample outside of these axis boundaries. The galaxies which are not detected in the observed $V-$ or $g-$ band (approximately rest-frame NUV) with 3σ are shown as open points; the rest frame colours of these galaxies are modest extrapolations of SED fits to redder photometry.
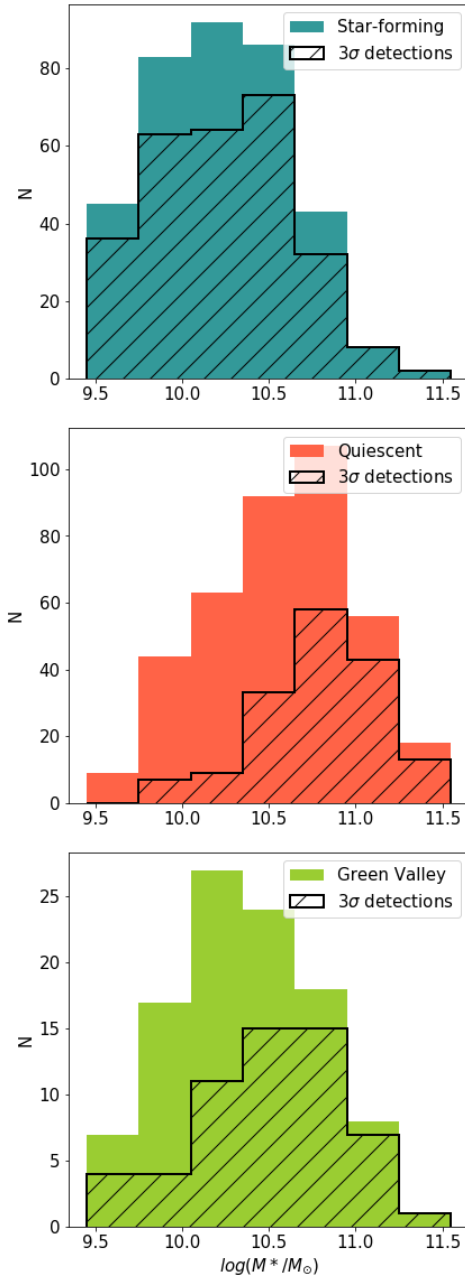
Figure 2.2: The fraction of galaxies that are detected (at $> 3\sigma$) in either the g or V band filters, for each population. These filters are close to the rest-frame NUV at the redshifts of interest.

Table 2.2: The rest-frame colour selections defining each of the main galaxy populations considered in this paper.

Population	Selection Criteria
Star-forming	$(NUV - V) < 2(V - J) + 1.1$
Quiescent	$(NUV - V) > 2(V - J) + 1.6$
Green Valley	$2(V - J) + 1.1 \leq (NUV - V) \leq 2(V - J) + 1.6$

Muzzin et al. (2013b) and van der Burg et al. (2020). Morever we have confirmed that, beyond 1 Mpc, there is little change in the fraction of each galaxy population with increasing radius. Thus we do not expect our results are sensitive to the definition of the reference field sample. Since the photometric redshift cut is wide, driven by the uncertainties on those redshifts, a statistical background subtraction is required for the cluster population even after this selection. We follow the method of van der Burg et al. (2013), where a correction factor is applied to the photometric sample in each radius or mass bin i, as:

$$\text{corr}_i = \frac{N_{i,\text{ secure cluster}} + N_{i,\text{ false negative}}}{N_{i,\text{ secure cluster}} + N_{i,\text{ false positive}}}, \tag{2.1}$$

where $N_{i,\text{ secure cluster}}$ are photometrically-selected and spectroscopically confirmed cluster members, $N_{i,\text{ false negative}}$ are spectroscpically confirmed cluster members that lie outside the ± 0.16 photometric redshift selection, and $N_{i,\text{ false positive}}$ are galaxies that lie within the photometric redshift range but are spectroscopically confirmed to be foreground or background galaxies. Note that, throughout this paper, the correction factor is always computed for the bins in radius and/or stellar mass that are being considered. This factor ranges from a value of 6 at low masses, to 0.5 at high masses.

Chapter 3

Results

3.1 Radial Distributions

We first consider how the fraction of galaxies in each population varies with environment, in Figure 3.1. Uncertainties on the measurements are obtained from 1000 bootstrap samples of our galaxy populations. As expected, we see an increase in star-forming galaxies with radius, and a decrease in the fraction of quiescent galaxies. Overall the cluster population shows a highly significant excess of quiescent galaxies, and corresponding deficit of star-forming galaxies, relative to the field. The composition of the field population, defined from galaxies in our catalogues at distances greater than 1 Mpc from the cluster centre, is not sensitive to how this population is defined, and our measurements are consistent with those based on the Ultravista survey (Muzzin et al., 2013b; van der Burg et al., 2020). On the other hand, the fraction of galaxies in the green valley population does not show a significant trend with radius, or display an excess in the cluster, compared to the field. Relative to the star-forming population, cluster cores do show an excess of green-valley galaxies. While we have noted above that some of this population may correspond to quiescent galaxies that have been misclassified due to uncertainties in their rest-frame colours, the fact that the two populations have very different radial distributions suggests that this effect is not dominant.
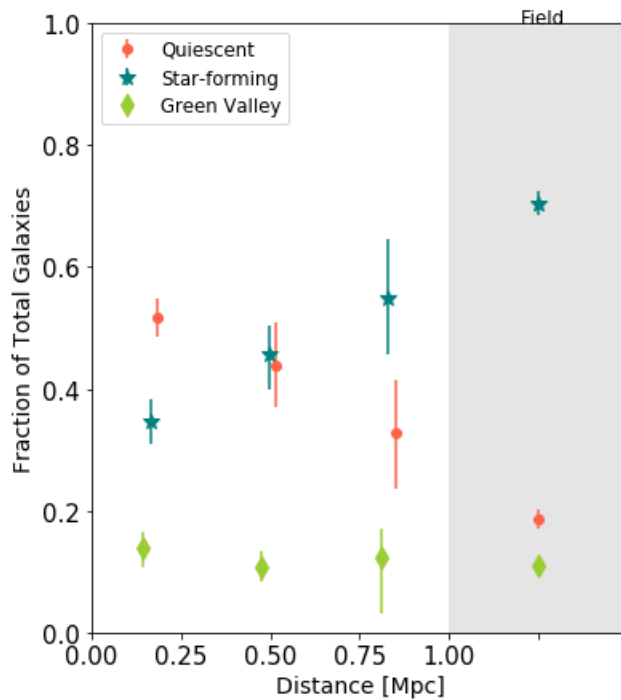
Figure 3.1: The fractions of each galaxy population are shown in bins of cluster centric radius, relative to the total population. The cluster population is taken here to be within 1 Mpc. The comparison field is given by the points shown in the grey region, and includes all the galaxies at $1 < z < 1.5$ beyond 1 Mpc. Here the green valley fractions do not appear to change with radius, and are consistent with the value for the field, indicating no environmental excess.

3.2   Stellar Mass Functions

The stellar mass functions for the quiescent, star-forming and green valley population in the cluster (< 1Mpc) and field populations are shown in Figure 3.2. Uncertainties assume Poisson statistics and do not include any uncertainty associated with the correction factor in Equation 2.1. We fit the data with Schechter functions of the form

$$\phi(M) = \frac{dN}{dM}dM = \phi^* \left(\frac{M}{M^*}\right)^\alpha \exp\left(-\frac{M}{M^*}\right) dM. \tag{3.1}$$

or, for $x = \log_{10} M/M_\odot$ as plotted in the Figure,

$$\phi(M) = \frac{dN}{dx}dx = \ln 10 \left(\frac{dN}{dM}\right) M dx =$$

$$= \ln 10 \phi^* M^* \left(\frac{M}{M^*}\right)^{1+\alpha} \exp\left(-\frac{-M}{M^*}\right) dx. \tag{3.2}$$

The normalization parameter, ϕ is fixed by forcing the integral to match the sum of the data where $\log(M/M_\odot) \geq 9.5$; the other two parameters are fit by minimizing the χ^2 statistic. The resulting fit parameters are given in Table 3.1. We show the 68 and 95 percent confidence ranges of M^* and α for the cluster population in Figure 3.3. The fit parameters of the star-forming population are consistent with those of van der Burg et al. (2020), as shown in Figure 3.3. For the quiescent population we find a larger $\log M^*$ and somewhat steeper (more negative) slope α than van der Burg et al. (2020). This is likely a consequence of the fact that much of the green valley population would be identified as quiescent in UVJ colour space (see Figure 4.6). For the field sample, the SMFs of the star-forming and quiescent populations agree fairly well with Muzzin et al. (2013b), though a deficit of bright star-forming galaxies yields a significantly lower M^*. This may in part be due to the inclusion of the intermediate green valley population; the shape of the total SMF is fully consistent with Muzzin et al. (2013b). As found by van der Burg et al. (2020), we find no significant difference in the shapes of the star-forming or quiescent galaxy mass functions between the cluster and field environments.

We now consider the mass function of the intermediate, green valley population. In both the cluster and field environments, the shape of the green valley SMF is intermediate between that of the star-forming and quiescent populations, but closer to that of the quiescent population. Though the parameters are not tightly constrained (shown for the cluster environment in Figure 3.3), the faint end slope is flat, $\alpha > -1.0$ with 2σ confidence.
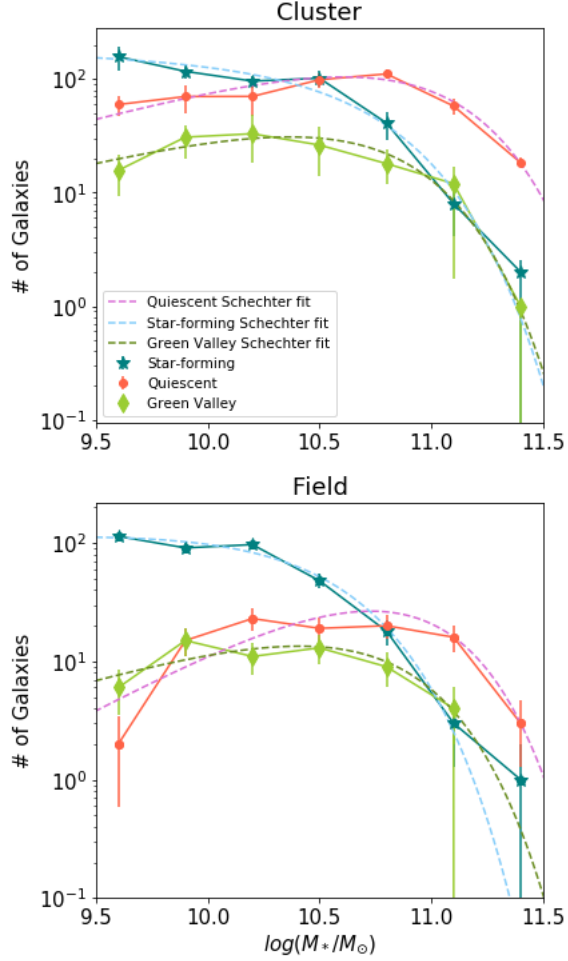
Figure 3.2: The mass functions for the star forming (blue), quiescent populations (red), and green valley (green), for both cluster and the field, compared with the Schechter functions shown as dashed lines calculated using Equation 3.1. Our mass functions for these populations are similar to those found in van der Burg et al. (2013), and the same difference in the shape of the SMF between the cluster and field for the quiescent population are displayed in the fits as well. The values for the Schechter fits are shown in Table 3.1.
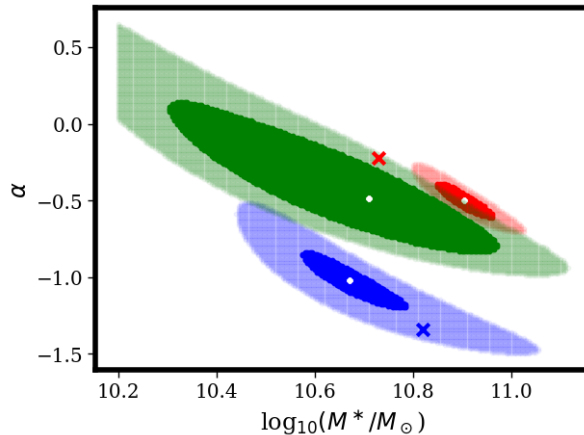
Figure 3.3: We show the 68 (dark) and 95 (light) percent confidence limits on the M^* and α parameters of our Schechter function fits to the cluster (< 1Mpc) population, for quiescent (red), star-forming (blue) and green-valley (green) galaxies. The white dots represent the best fit. The crosses are the best fit parameters to the quiescent and star forming populations (defined in UVJ space, without a green valley) by van der Burg et al. (2020)

It is therefore unlikely that the majority of this intermediate population can be made up of galaxies transformed directly from the infalling star-forming population, without significant change in stellar mass. This complicates the interpretation of the population ratios in Figure 3.1. For example, the transition rate cannot be determined simply by comparing the abundance of green valley galaxies to that of the star–forming population; we instead need to account for all routes into and out of the green valley, as a function of stellar mass. We therefore turn to a simple framework to determine the rates timescales associated with galaxies transiting through the green valley, based only on observations of the SMFs.

3.3 Transition Timescales

Inspired by the approach of Socolovsky et al. (2018), we can now use our measurements of the green valley population to gain some insight into any environment-related transformation of galaxy properties at $1 < z < 1.5$. We will assume that a galaxy's star formation history is determined only by its present day stellar mass and/or its environment. For the latter we consider only the cluster and field environments.
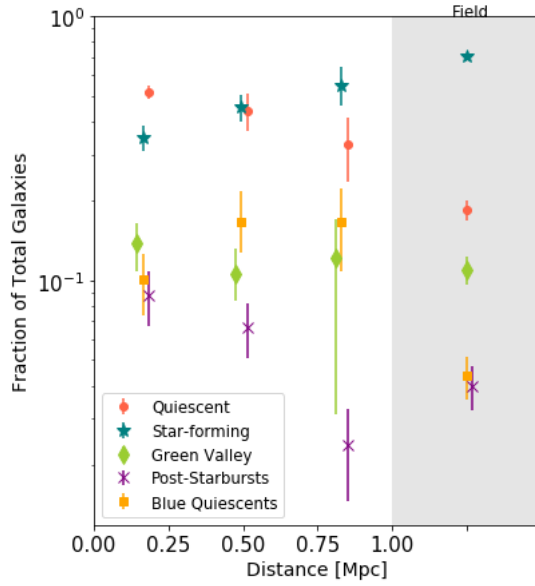
Figure 3.4: The relative abundance of various populations are shown as a function of clustercentric distance. The NUV-J defined populations of star-forming, quiescent, and green valley, are defined as in Figure 2.1. Blue Quiescent Galaxy (BQG) population is defined as the blue end of the red sequence in UVJ colour space, and the spectroscopic sample of "post-starburst" galaxies (PSBs), are defined based on their D4000 and [OII] indices. For the PSBs we are comparing their abundance relative to the total spectroscopic members, where the other populations are compared to the total photometric members. The BQG population shows the largest excess relative to the field; in all three cases any trend with cluster-centric radius is weak.

17

Table 3.1: The values for the two-parameter Schechter mass function fits, for each of the galaxy populations in both the cluster and the field. The values in this table correspond to the parameters in Equation 3.1, and are used to plot the SMF fits shown in Figure 3.2. For the purpose of re-creating these fits, the normalization for the total field ($\phi^*_{\text{ref}} = \phi^*_{\text{tot,field}} = 1.91 \times 10^{-9}$) is used as a reference for the relative normalizations shown here.

		χ^2	$log_{10}(M^*/M_\odot)$	α	$\phi^*/\phi^*_{\text{ref}}$
	SF	6.42	$10.69^{+0.1}_{-0.11}$	$-1.05^{+0.21}_{-0.15}$	0.66
r <1 Mpc	Qui	3.36	$10.90^{+0.07}_{-0.04}$	$-0.50^{+0.1}_{-0.13}$	0.72
	GV	1.58	$10.71^{+0.28}_{-0.39}$	$-0.49^{+1.85}_{-0.31}$	0.33
	Total	10.91	$10.96^{+0.075}_{-0.06}$	$-0.88^{+0.04}_{-0.15}$	0.83
	SF	4.92	$10.48^{+0.1}_{-0.08}$	$-0.92^{+0.14}_{-0.13}$	1.11
Field	Qui	11.58	$10.72^{+0.11}_{-0.12}$	$0.03^{+0.23}_{-0.19}$	0.31
	GV	2.35	$10.64^{+0.26}_{-0.28}$	$-0.42^{+0.51}_{-0.38}$	0.16
	Total	7.20	$10.65^{+0.07}_{-0.09}$	$-0.85^{+0.08}_{-0.07}$	1

18

Figure 3.5: The transition rate factors, including $\gamma(M)$, $\beta(M)$, and $\tau(M)$, describing the transition of field galaxies (bottom row) and cluster galaxies (top row) into each of the cluster populations: star-forming (SF), green valley (GV) and quiescent (Qui). These three parameters are all a function of mass. The way these parameters correspond to the transitioning populations are shown in Equations 3.5–3.16. The arrow indicating $\beta(M)$ goes from the SF population to Qui, passing through the GV population, where the dashed line shows that the galaxies can spend an amount of time (τ) there before continuing their transition. The dotted arrows here show pathways for transition between the field populations that we expect to exist, but that we are not attempting to constrain in this work. This image depicts a snapshot in time and what transitions are happening, but we also use the model to calculate β averaged over the cluster lifetime (β_{avg}).

We construct a framework where the galaxy population in clusters is built by modifying ("transforming") galaxies from the field at the same redshift. This transformation can have occurred at any time in the past, and includes the case where a unique population or sub-population of galaxies pre-existed in the protocluster. It simply quantifies what changes need to be made to match the cluster galaxy population, over and above the evolution that leads to the average galaxy population at the same redshift.

Our framework is described in Figure 3.5. We assume the total cluster stellar mass function $\phi^C(M)$ is built up from the field, $\phi^F(M)$ at a rate $\gamma(M,z)\phi^F$, where M is the final stellar mass of the galaxy, at the redshift of observation. Thus, writing as a function of time t rather than redshift,

$$\frac{d}{dt}\phi^C(t) = \gamma\phi^F(t) \tag{3.3}$$

or

$$\gamma = \frac{1}{\phi^F(t)}\frac{d}{dt}\phi^C(t) \tag{3.4}$$

The average value of γ can be computed simply by taking $\Delta t = T$ to be the age of the Universe and setting $\phi^C(0) = 0$, as appropriate if the entire cluster population has been built in this way. Thus,

$$\gamma(M) \approx \frac{1}{\Delta t}\frac{\Delta\phi^C(M)}{\phi^F(M)} \approx \frac{1}{T}\frac{\phi^C(M)}{\phi^F(M)} \tag{3.5}$$

Now we assume that there is some process that preferentially quenches star formation in cluster galaxies. We characterize this with the parameter $\beta(M,z)$, which represents the fraction of star-forming galaxies that stop forming stars (at a rate sufficient to be classified as SF), per unit time. Necessarily, these galaxies must then become green valley galaxies. This quenching applies both to existing SF galaxies in the cluster, as well as to any SF galaxies accreted from the field in timestep dt. We next assume that galaxies quenched in this way remain as green valley galaxies for a time $\tau(M)$, before their colours evolve sufficiently that they are classified as quiescent. Coupled with the direct accretion (at rate γ) of green valley and quiescent galaxies from the field, this completes the model schematic shown in Figure 3.5. Note that we have said nothing about the mechanisms that transform galaxies within the field population; by simply using the observed field stellar mass functions at the time of observation the model accounts for that evolution without needing to parameterize it. This is a feature of our approach.

20
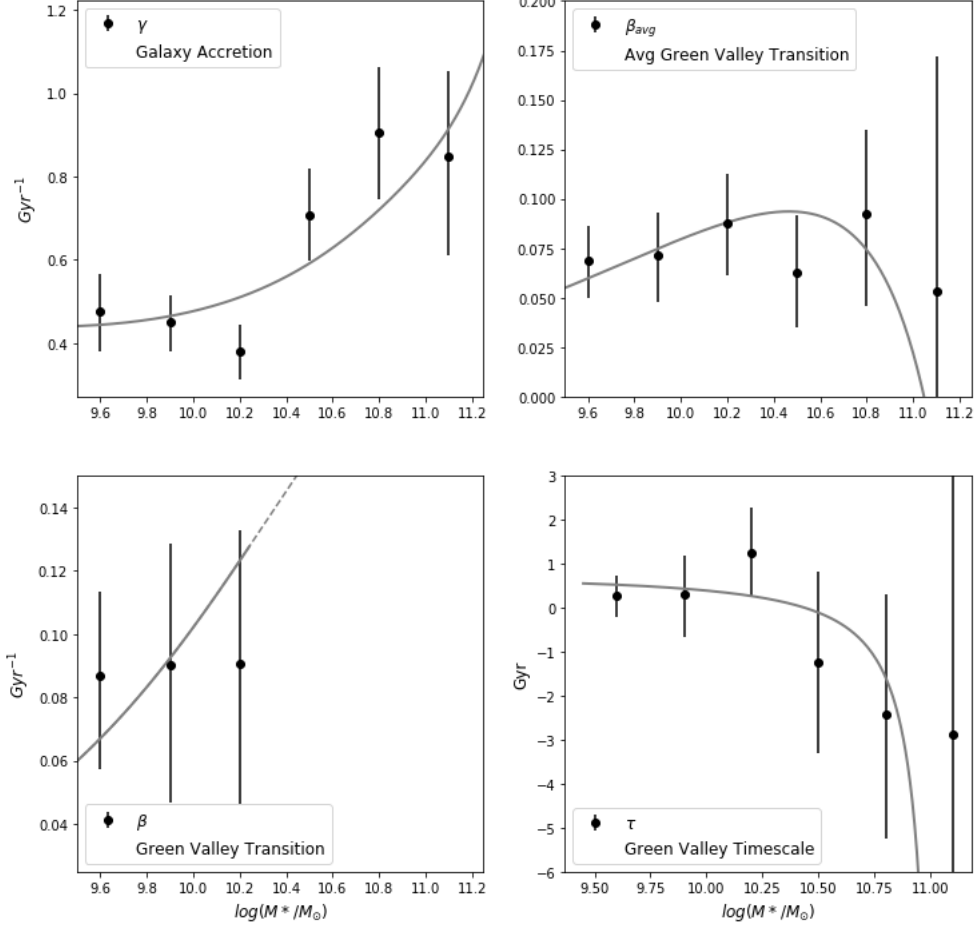
Figure 3.6: The transition parameters as a function of mass as described in Equations 3.5, 3.11, 3.14 and 3.16, and shown graphically in Figure 3.5. γ describes the transition from the field to the cluster (green), and β describes the transition through the green valley in between the star forming and quiescent populations. We also compare the transition rate β to the average over the cluster lifetime (β_{avg}) which we have estimated at 4 Gyr, where we do not see a significant difference between this past average and the current instantaneous transition rate (Figure 3.7). Smooth curves are derived from the Schechter function fits to the stellar mass functions. The dotted line represents the region where the fit is poorly constrained by the data, which have error bars larger than the scale of the figures and are not plotted here.
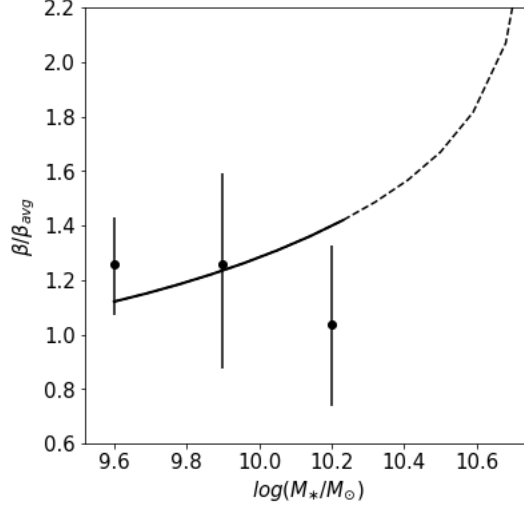
Figure 3.7: The ratio of the current to past average environmental quenching rate, $\beta(T)/\beta_{avg}$. The points represent the measurements and the lines are derived from the Schechter function fit parameters, where the dotted line represents the region where the fit is poorly constrained by the data.

We now proceed to evaluate the other parameters of the model. All the parameters and the mass functions ϕ are mass dependent; for clarity we don't write the mass dependence of ϕ explicitly in the following equations. The quenching rate, $\beta(M)$, can be determined just by comparing the SMF of SF galaxies in the cluster and field (ϕ_S^C and ϕ_S^F, respectively). With reference to Figure 3.5 we write:

$$\frac{d\phi_S^C}{dt} = \phi_S^C(t + dt) - \phi_S^C(t) \tag{3.6}$$

$$= \gamma\phi_S^F(t)dt - \beta(M)\phi_S^C(t)dt - \gamma(M)dt\phi_S^F(t)\beta(M)dt. \tag{3.7}$$

The three terms on the right hand side correspond to i) star-forming galaxies accreted directly from the field in time dt; ii) existing cluster star forming cluster galaxies that have been environmentally quenched in time dt; and iii) field star-forming galaxies accreted in time dt that would be environmentally quenched in that time. Simplifying,

$$\frac{d\phi_S^C}{dt} = \gamma(M)\phi_S^F\left[1 - \beta(M)dt\right] - \beta(M)\phi_S^C \tag{3.8}$$

22

Then we can calculate the average quenching rate ($\beta_{avg}(M)$) over the lifetime of the cluster (T):

$$\Delta\phi_S^C \approx \phi_S^C \approx \left[\gamma(M)\phi_S^F \left(1 - \beta_{avg}(M)T\right)\right] T, \tag{3.9}$$

where we have used the fact that, initially, $\phi_S^C = 0$. Solving this for $\beta_{avg}(M)$ gives

$$\beta_{avg}(M) = \frac{1}{T}\left[1 - \frac{1}{T\gamma(M)}\frac{\phi_S^C}{\phi_S^F}\right] \tag{3.10}$$

and after substituting for $\gamma(M)$ using equation 3.5 we have

$$\beta_{avg}(M) = \frac{1}{T}\left[1 - \frac{\phi^F}{\phi^C}\frac{\phi_S^C}{\phi_S^F}\right]. \tag{3.11}$$

We note that Equation 3.11 depends only on the relative fraction of star-forming galaxies in the cluster and field. The green valley is irrelevant for the average quenching rate. In fact, we show in Appendix B that β is simply related to the commonly used "Quenched Fraction Excess" (e.g. van den Bosch et al., 2008; Peng et al., 2010; Bahé et al., 2017; van der Burg et al., 2020):

$$\mathrm{QFE} \approx \frac{f_{\mathrm{NSF}}^C - f_{\mathrm{NSF}}^F}{1 - f_{\mathrm{NSF}}^F} = T\beta_{avg} \tag{3.12}$$

where f_{NSF}^C and f_{NSF}^F are the fraction of non-star forming (i.e. quiescent and green valley galaxies in our current classification) galaxies in the cluster and field respectively.

The green valley does, however, contain important information about the *recent* quenching rate, since galaxies quenched within time τ of observation will still exist in that population. We can write the observed green valley SMF as follows:

$$\phi_G^C \approx \gamma(M)T\phi_G^F + \phi_S^C\beta(M)\tau(M) + \left[\gamma(M)\tau(M)\right]\left[\beta(M)\tau(M)\right]\phi_S^F, \tag{3.13}$$

where ϕ_G^C and ϕ_G^F are the SMF of the green valley population in the cluster and field, respectively. The first term on the right hand side represents all the accreted galaxies that would be in the green valley after time T due to normal field evolution; this is the vertical line pointing from the field to cluster GV in Figure 3.5. The next two terms represent the environmentally quenched population, coming from both the existing cluster SF galaxies and the accreted field SF galaxies, integrated over the GV timescale τ. We can rearrange this to solve for β:

$$\beta = \frac{1}{\tau(M)}\left[\frac{\phi_G^C - \gamma(M)T\phi_G^F}{\phi_S^C + \gamma(M)\tau(M)\phi_S^F}\right] \tag{3.14}$$

23

This requires information about τ, which we obtain from the SMF of the Quiescent cluster population (ϕ_Q), following:

$$\phi_Q^C = \gamma(M)T\phi_Q^F + \gamma(M)T\beta_{avg}(M)\left[T - \tau(M)\right]\phi_S^F, \tag{3.15}$$

where the first term accounts for quiescent galaxies accreted directly from the field, and the second term corresponds to all the accreted, environmentally quenched SF galaxies that are not still in the GV. Thus, we obtain

$$\tau(M) = T - \left[\frac{\phi_Q^C - \gamma(M)T\phi_Q^F}{\gamma(M)T\beta_{avg}(M)\phi_S^F}\right]. \tag{3.16}$$

Using the equations above, we can use the observed SMFs to determine the stellar-mass dependent values of γ, β, β_{avg} and τ as a function of stellar mass, calculated from the observed $\phi(M)$ stellar mass functions. The results are shown in Figure 3.6, which includes the binned measurements and also smooth curves derived from the Schechter function fits to the SMFs. The parameter γ characterizes the difference between the total SMF in the cluster and field environments; we make the assumption that this is constant with time, and thus adopt the average value as calculated in Equation 3.5. The overall normalization is irrelevant, since the field and cluster SMFs themselves are arbitrarily normalized. However the dependence of γ on stellar mass reflects the difference in the shape of the SMF is between clusters and the field (see also van der Burg et al., 2020). Otherwise, its interpretation is not of great importance for the present purpose. The average quenching parameter, β_{avg}, has a value of ~ 0.08 per Gyr (somewhat larger in the cluster cores). This is consistent with the QFE~ 0.4 that we measure (van der Burg et al., 2020), given Equation 3.12. We do observe a weak stellar mass dependence of β_{avg}, though this is weaker than found by van der Burg et al. (2020). A stronger trend with stellar mass is seen if we limit the analysis to the central 0.5 Mpc, as shown in Appendix A.

Our analysis of the green valley population sheds new light on this through the parameters τ and $\beta(T)$. Although the uncertainties are large, we find τ is generally small, consistent with zero and < 1Gyr on average. This is what we would expect for rapid, cluster-induced quenching mechanisms like ram-pressure stripping. Note that only a fraction of green valley galaxies are a result of this cluster-driven quenching process; we return to this in § 4. With the way we have defined our transition parameters, we are not only considering a uni-directional flow from the star-forming sequence to quiescence. In particular, a negative value of $\tau(M)$ represents a population of green valley galaxies in excess of what can be attributed to transitioning star-forming galaxies, effectively describing a flow from the quiescent sequence into the green valley.

Finally we consider our estimate of $\beta(T)$, the quenching rate at the epoch of observation, (averaged over the short timescale τ). This parameter is only well constrained for $M < 10^{10.5} M_\odot$, and we do not plot the data at larger masses since the uncertainties are larger than the size of the figure. Over this mass range, $\beta(T)$ is comparable in magnitude to β_{avg}, which we demonstrate more directly in Figure 3.7. If anything the current quenching rate may be somewhat *higher* than the past average, especially in the cluster cores. This is apparently at odds with the interpretation of van der Burg et al. (2020) and Webb et al. (2020), who argue that most of the environmental quenching must have happened early, in protoclusters. We will return to this point in § 4.4.

Chapter 4

Discussion

In this paper we have taken advantage of deep rest-frame NUV photometry to identify transition galaxies in the green valley between the dominant star-forming and quiescent populations. The advantage of our particular definition is that it captures any transitioning galaxies, regardless of their mass, dust content or other properties. The disadvantage is that the population is not "pure" but will contain, for example, galaxies with low but slowly declining star formation rates, edge-on dusty galaxies, or predominantly quiescent galaxies that have been modestly rejuvenated through gas rich mergers (e.g. Schawinski et al., 2014; Vulcani et al., 2015). By comparing the populations in the cluster to that of the general field, we are able to statistically isolate a population that is in the green valley as a result of the cluster environment. In our simple model, where star-forming galaxies in the cluster are quenched at a rate $\beta \sim 0.08/\text{Gyr}$ and exist in the green valley for a time $\tau \lesssim 1$ Gyr, we can determine that the fraction of SF galaxies presently in the green valley as a direct result of environment quenching should be $\beta\tau < 0.1$. From Figure 3.1 we see that the total green valley population represents about 10 per cent of the total population while the SF fraction is about 50 per cent. This means the green valley is ~ 20 per cent of the SF population. Thus, we expect that less than about half of these galaxies are the result of environment quenching.

We now compare with two alternative ways to identify transition galaxies. These are complementary, as they aim to select a more pure sample of transition galaxies, at the expense of being (likely) incomplete. The first definition is a photometric selection of galaxies at the blue end of the quiescent population identified in UVJ colour space. This has been advocated by, for example, Belli et al. (2019) who use deep rest-frame optical spectroscopy of 24 quiescent galaxies at $1.5 < z < 2.5$ to demonstrate that galaxies in this part of colour space are distinctly younger than most of the quiescent population. While
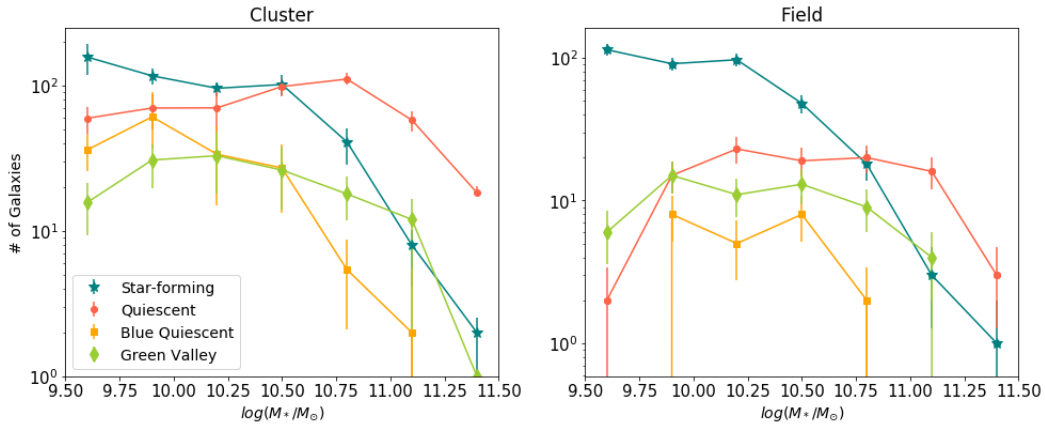
Figure 4.1: The stellar mass functions for the BQG population in the Cluster and Field is compared with our thee primary populations (star forming, green valley and quiescent). The BQG galaxies are identified as the blue-end of the red sequence, in UVJ colour space, while the other three are defined in NUV-V-J space as described in the text. The BQG population shows a steep faint end slope, more similar to the star-forming population than the quiescent.

Belli et al. (2019) and others refer to these as "post-starburst" galaxies, we prefer a more model-independent term, and will call them "Blue Quiescent Galaxies" (BQGs). They argue that galaxies passing through this space are a result of relatively fast quenching; assuming that dust disappears immediately after star formation stops, such galaxies will be very blue for a short time, until the remaining massive stars die out.

The second is a spectroscopic definition, based on the D4000 and [OII] indices (Muzzin et al., 2014). Galaxies with blue colours (D4000<1.45) and undetected [OII] emission, are identified as candidate post-starburst (PSB) galaxies. In the following sections we identify both types of transition galaxies, and compare them with our green valley selection. We show the radial distributions (Figure 3.4), and mass functions (Figure 4.1) of these populations along with the ratio of the total stellar mass functions for each population (Figure 4.2).
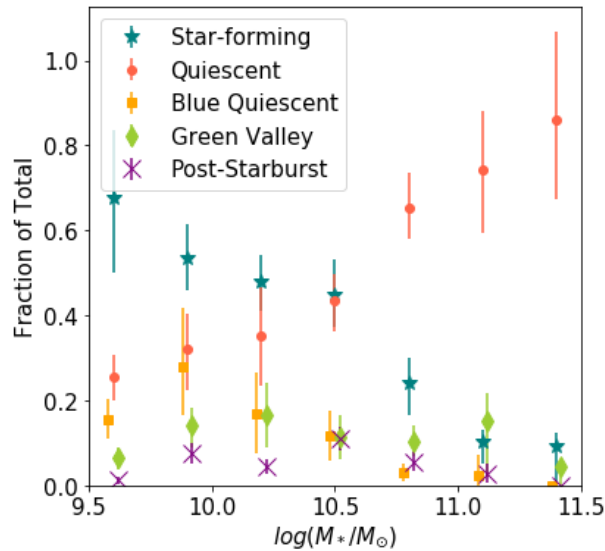
Figure 4.2: The ratio of the mass functions for each cluster population compared to the total mass function. Here only the total SMF of the spectroscopic members is used to compare with the post-starburst population.

4.1   Blue Quiescent Galaxies

We reproduce the Belli et al. (2019) selection of blue quiescent galaxies, as shown in Figure 4.3. The selection box definition is

$$(V - J) + 0.45 \leq (UV - V) \leq (V - J) + 1.35 \tag{4.1}$$

$$-1.25(V - J) + 2.025 \leq (UV - V) \leq -1.25(V - J) + 2.7. \tag{4.2}$$

Figure 4.3 also shows the mass-weighted ages of galaxies we identify as quiescent based on their NUV colours (as in § 3). The ages are measured by fitting the photometry with FAST (as described in van der Burg et al., 2020), giving the age at which star-formation starts (Kriek et al., 2009). We confirm that these galaxies are typically younger than the rest of the quiescent population; the result is not as striking as in Belli et al. (2019), but our age measurements are not likely as precise, either.

The fraction of BQG galaxies in our sample is shown as a function of clustercentric radius, in Figure 3.4. They make up 10–20 per cent of the cluster population, significantly in excess of their relative abundance in the field at < 5 per cent. The latter is consistent with what Belli et al. (2019) find at similar redshifts.
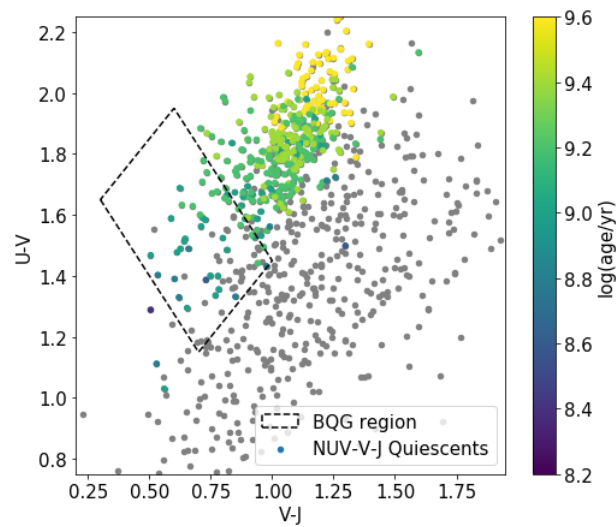
Figure 4.3: We show our cluster galaxy sample in (U-V) vs (V-J) colour space. Galaxies classified as quiescent (based on the NUV-J diagnostic) are coloured by their age, as determined from SED fitting with FAST. An age gradient along the quiescent sequence is apparent. The BQG selection is drawn as in Belli et al. (2019) around the galaxies at the blue end of the quiescent population, shown by the dashed box.
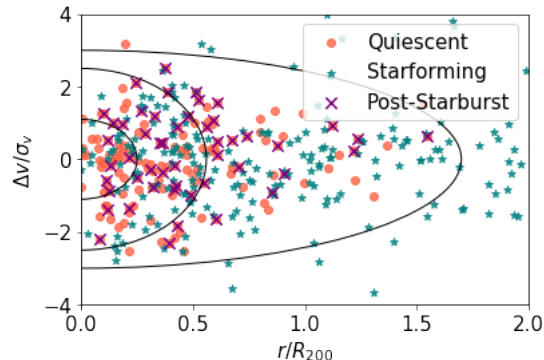
Figure 4.4: The distribution of PSB galaxies in phase space, as defined by Muzzin et al. (2014). The post-starburst galaxies here are selected spectroscopically in the same way, using the D4000 break and the OII emission. Using the same phase space contours (black lines), we do not find the same inner phase space bin deficit- since we still see PSBs within the inner most contour.

We show the stellar mass function of our BQG population in Figure 4.1. This is compared with our three primary populations from Figure 3.2. Note that the BQG population is not independent of the others, as it is defined in UVJ space while our primary populations are defined in NUV-V-J space. The sample of BQGs is small, so the shape of the SMF is not very well constrained, especially in the field. However, unlike the green valley population, its shape is statistically consistent with that of the star-forming galaxies within 1σ, with a steep faint end slope. It is inconsistent with the parameters of the quiescent galaxy SMF. This supports an interpretation in which most of the BQGs arise from rapid quenching of the star-forming galaxies. In that case, the contrast with the field is even more striking, as the abundance of BQGs is about 30% that of the normal SF population in clusters, but only $\sim 5\%$ in the field.

4.2   Spectroscopic Post-starburst Galaxies

Post-starburst galaxies were first identified spectroscopically by Dressler & Gunn (1983), as galaxies with strong Balmer (specifically $H\delta$) absorption and weak nebular emission ([OII]). As shown for example by Couch & Sharples (1987), the most extreme examples of these galaxies require a burst of star formation followed by rapid truncation to explain the spectrum dominated by A-stars. As Balmer absorption is difficult to measure reliably in low signal-to-noise ratio spectroscopy, Muzzin et al. (2012) adopt a different definition,
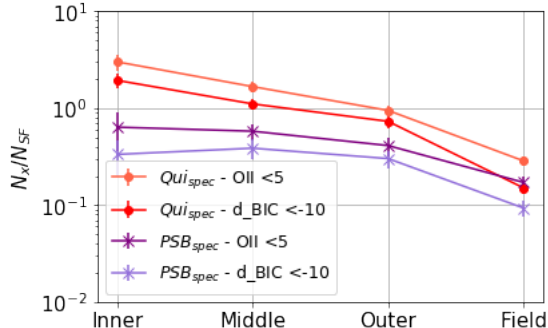
Figure 4.5: The number of quiescent and spectroscopic PSB galaxies, relative to the number of star-forming galaxies, are shown as a function of phase space bins. Bins are chosen as in Muzzin et al. (2014) and shown in Figure 4.4. We do not observe a strong trend in abundance with phase space.

based on D4000. Galaxies with D4000< 1.45 are dominated by young stars, but a lack of [OII] emission again indicates no ongoing star formation. We identify the absence of [OII] emission using the Bayesian Information Criterion (BIC), where model fits without an emission line are strongly preferred (BIC< −10), as described in Old et al. (2020). Our final definition is then:

$$(\mathrm{D4000} < 1.45) \cap (\Delta_{\mathrm{BIC}} < -10) \tag{4.3}$$

The relative abundance of these galaxies, compared to the total spectroscopic members is shown in the right panel of Figure 3.4. They are the least abundant of all the populations we have identified, at $\sim 7.4 \pm 1.4$ per cent of the cluster. This is a factor of $\sim 2.5 \pm 1.3$ times larger than the field value, in good agreement with the measurements of Muzzin et al. (2012) for similarly selected clusters at slightly lower redshift ($0.8 < z < 1.3$), integrated over the full stellar mass range.

To compare more directly with Muzzin et al. (2014) we show the distribution of spectroscopic post-starburst galaxies in position-velocity phase-space, in Figure 4.4. This is possible only for this spectroscopic sample, for which we calculate the velocity offset relative to the cluster centre. For consistency we redefine the star-forming and quiescent spectroscopic sample using the D4000 index, in the same way as Muzzin et al. (2014); note this differs from the NUV-V-J definition we used for our main analysis in § 3. Our results are broadly consistent with those of Muzzin et al. (2014). We divide phase space into three regions following their same definition, and present the fraction of PSB and quiescent galaxies relative to the star-forming population in Figure 4.5. We find broad agreement, as the PSB abundance drops from ~ 20 per cent in the cluster core to < 5 per
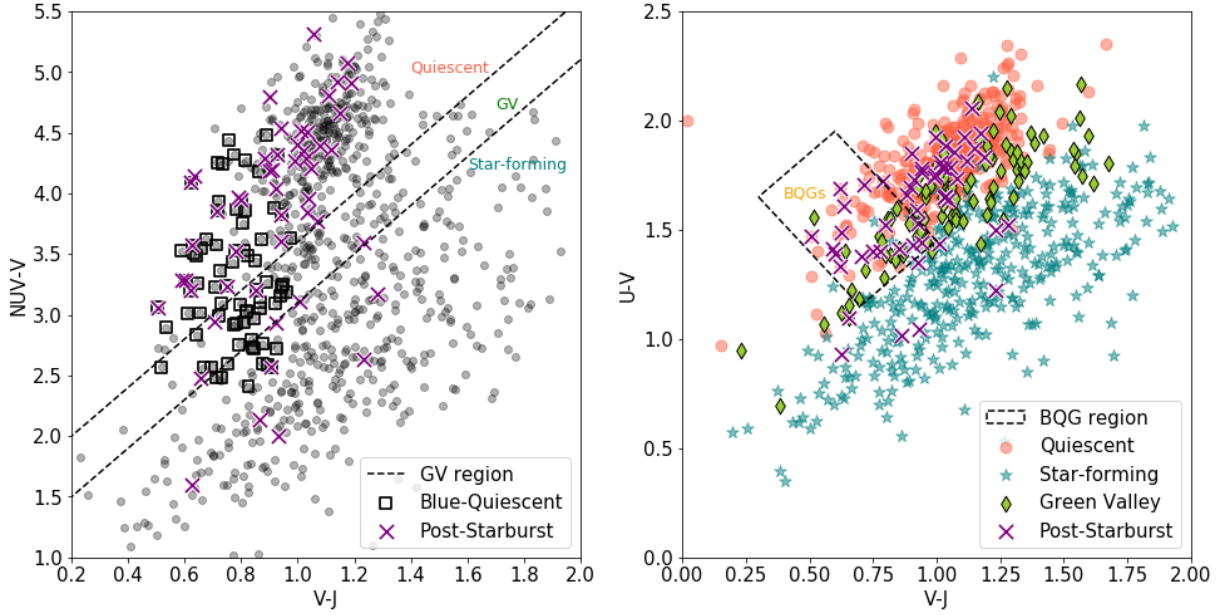
Figure 4.6: The *left panel* shows our sample in the NUV-V-J colour plane that we use to define our primary Quiescent, Star-forming and green valley populations, as in Figure 2.1. The BQGs (black squares) are selected in U-V V-J space, where we select out the blue end of the red sequence shown by the dashed box in the *right panel*, making this selection not independent of the others. The spectroscopic post-starbursts (purple crosses) are selected by their OII emission and D4000 break (shown in Figure C.2) and are also not independent of the photometric selections previously described.

cent in the field. However, we do not observe the same sharp drop in abundance in the inner and outer phase space bins noted by Muzzin et al. (2014). We have checked that the result does not change if we adopt a less strict selection for the absence of [OII] (rest-frame equivalent width < 5Å), as shown on the Figure. Therefore, while we confirm an excess of PSB galaxies in the dense cluster environment, we do not find evidence that they are clustered in a specific region of phase space.

4.3 Interpretation: the different phases of transition

The first question is to what extent these three candidate transition populations – the green-valley, BQG and spectroscopic PSB – overlap. We first consider their overlap in colour space, in Figure 4.6. What is immediately apparent is that the three populations are somewhat distinct. In particular, the green valley as we have defined it contains a few BQGs, but almost no spectroscopic PSBs. The BQGs and PSBs have a greater degree of overlap, though the former is more tightly confined in colour space, as required given the definition.

In general many of the spectroscopic PSB galaxies are quite red in NUV-V or U-V colours, which is somewhat surprising given their definition based on D4000 (itself similar to a U-V colour). We show this explicitly in Figure 4.7. The red PSB galaxies do have correspondingly large D4000, and in fact are clustered close to the threshold used to define them. Modestly adjusting the definition to D4000 < 1.4 would remove many of these red galaxies. This particular definition may therefore somewhat overestimate the fraction of true PSB galaxies. Finally, we compare the available spectra of each galaxy type, in Figure 4.8. We normalize the spectra to the wavelength range $4000 < \lambda/$Å< 4100 and combine them weighted by the inverse variance. All selections exhibit the strong absorption lines characteristic of young stellar populations. Both the green valley and BQG populations show weak [OII] emission in the stacked spectrum, which could indicate residual star formation but would also result from a somewhat heterogeneous population that includes some star–forming galaxies.

The results are approximately consistent with the following picture. The spectroscopic PSB phase is the longest-lived, and thus captures galaxies in both the blue (star-forming) and red (quiescent) parts of the NUV-V-J diagram. This relatively long lifetime is at least partly a consequence of the specific definition, which includes galaxies with fairly large D4000 and with some residual star formation (given the reliance on [OII] detection in low S/N spectra). Galaxies transition through the blue end of the green valley fairly rapidly, on timescales < 1 Gyr, entering the BQG phase before finally becoming red. Muzzin
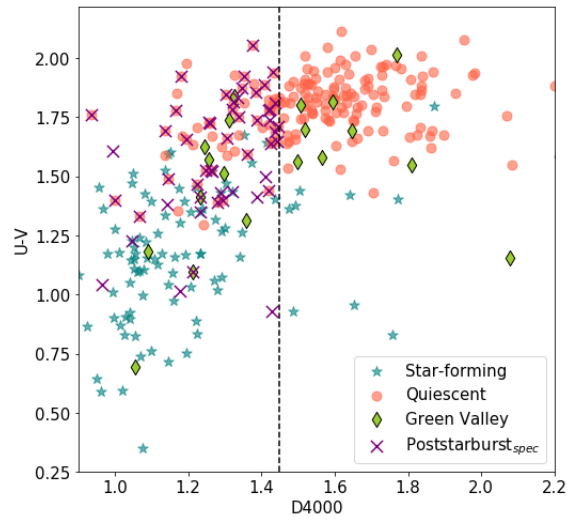
Figure 4.7: The U-V colour of our cluster galaxies are shown as a function of the D4000 spectral index. There is a good correlation, and our quiescent and star-forming galaxies are largely separable in both quantities. The spectroscopic post-starburst sample is intermediate, and in particular includes several galaxies at the red boundary of the D4000 definition (1.45), with U-V colours more typical of the quiescent population.
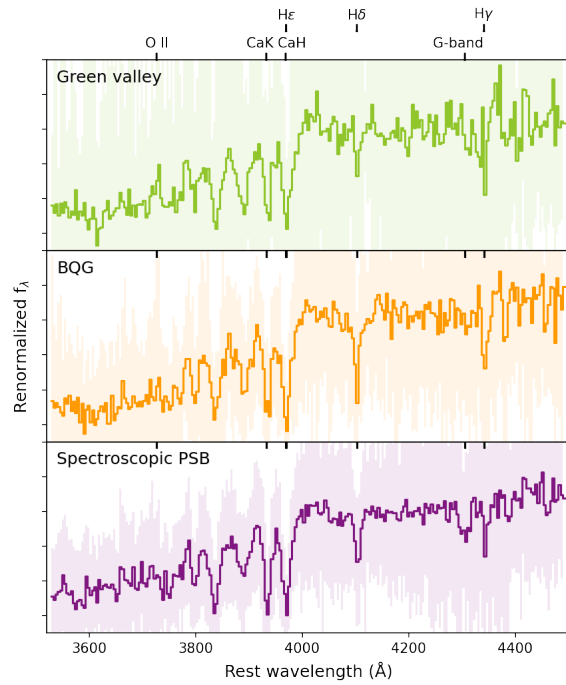
Figure 4.8: Median-combined spectra for galaxies in the Green valley, BQG or Spectro-scopic PSB categories considered in the text. Spectra are normalized just redward of the 4000Å break. All three exhibit strong Balmer and other absorption lines. [OII] emission is weak but clearly present in both the BQG and Green valley samples.

et al. (2012) find the average spectrum of their PSB sample can be explained by a SFR that declines linearly to zero over a time $t_{PSB} = 0.4^{+0.3}_{-0.4}$Gyr. The uncertainties on this value and our own measurement of τ are too large to reach any strong conclusions, but are at least consistent with this interpretation that $t_{PSB} > \tau$. The current quenching rate that we would infer from the PSB population, adopting the above value of t_{PSB}, is that $\sim 10/t_{PSB} \approx 0.25 \pm 0.25$ per cent of spiral galaxies are quenched every Gyr. This value is statistically consistent with our corresponding measurement of β, though again the uncertainties preclude a more detailed comparison.

There is some overlap between the BQG population and the blue end of the green valley. Cluster BQGs make up ~ 15 per cent of the total; this is comparable in size to the subset of green valley galaxies that our analysis indicates are undergoing environment-driven transformation (i.e. ~ 10 per cent of the total population). This, coupled with the low value of τ that we find, suggests most of this environment-driven transformation is via the fast-quenching ($\tau \sim 100$ Myr) mode described by Belli et al. (2019). Of course galaxies may still be passing through the green valley via slow quenching, but at a rate that is not strongly environment dependent.

4.4   Environment quenching in GOGREEN

We have shown that the green valley, spectroscopic PSB and BQG populations are all consistent with an environment-driven quenching rate in the GOGREEN clusters that is comparable to the past average quenching rate. This is naively at odds with the results of van der Burg et al. (2020) and Webb et al. (2020). In the former case, it was noted that the environment-independence of the quiescent galaxy SMF is difficult to reconcile with it being built significantly from quenching star-forming galaxies (which have a much steeper SMF). In Webb et al. (2020) it was found that the mass-weighted ages of cluster and field quiescent galaxies are comparable; if anything, cluster galaxies are somewhat older. This is also inconsistent with a scenario in which a significant fraction of cluster galaxies have been recently quenched, prematurely relative to similar mass galaxies in the field.

The van der Burg et al. (2020) result can be accommodated if environmental quenching has a similar dependence on stellar mass as does the environmentally-independent quenching that affects the field population. This could be coincidental, or because the underlying mechanism is the same in both cases. For example, gas exhaustion might be the driving factor in both cases, accelerated in clusters where gas accretion from the cosmic web is truncated (e.g. McGee et al., 2014). There is no fundamental need for that quenching to occur exclusively in protoclusters. The lack of an age difference with environment could be

reconciled if pre-processing is important; i.e. if environmental quenching is initiated when galaxies first become satellites, long before they are accreted into more massive clusters. Analysis of GOGREEN systems as a function of halo mass supports this interpretation (Reeves et al. in prep).

We therefore conclude that the only notable difference between environmental quenching at $1 < z < 1.5$ and lower redshift is that this process is stellar mass dependent at the higher redshift, but apparently independent of stellar mass at low redshift. One possible explanation could be that quenching associated with mergers plays a role at $z > 1$. We have neglected merging in our simple framework, and it would be interesting to consider its effect in future work.

Chapter 5

Conclusions

In this work we have split the galaxy sample of the GOGREEN clusters into different populations based on their NUV-V, V-J colours, in order to define an intermediate transition population, the green valley, between the star-forming and quiescent populations. Using this colour-colour space to define these populations allowed us to create a complete, though not pure transition population (Figure 1). Our main findings are as follows:

- Green valley galaxies were found to make up about 10 per cent of the cluster population, with no strong dependence on cluster-centric radius, and relatively consistent with the field population (Figure 3.1).

- Computing the stellar mass functions for each of the populations shows that the green valley is similar to that of the quiescent population, specifically in the flat faint end slope (Figure 3.2).

- We also use these stellar mass functions alongside a simple framework (Figure 3.5) to determine transition parameters for the green valley. Here we define a parameter β which defines the rate at which galaxies are quenched by their environment- entering the green valley and spending a period τ in the green valley before moving to the quiescent sequence. We find $\beta = 0.08/Gyr$ (Figure 3.6) which is consistent with the past average quenching rate, β_{avg} (Figure 3.7).

- We find τ consistent with zero Gyr, which is what we expect for rapid, cluster-induced quenching caused by mechanisms like ram-pressure stripping.

- The stellar mass function of the blue-quiescent galaxies resembles that of the star-forming population, and their fraction shows a large excess within the cluster compared to the field.

- The spectroscopic post-starbursts show a similarly large cluster excess when compared to the field, with a fairly strong radial dependence within the cluster.

- We do not see the same phase space dependence on the fraction of post-starbursts as Muzzin, so the physical driver of the fast-quenching resulting in these galaxies remains unclear

van der Burg et al. (2020), measuring the SMF and comparing with COSMO/ UltraVISTA field SMFs, find that the quenched fraction in clusters is higher than in the field at all stellar masses, and the quenched fraction excess (QFE) defined as the excess quenching due to cluster environment, is positive for all masses, but increases with increasing mass. The shapes of the SMFs in both the star-forming and quiescent populations are consistent with their field counterparts.

Webb et al. (2020), fitting rest-frame optical spectroscopy and photometry to stellar population models, determine the star-formation histories of the sample and using the SFHs compute the mass-weighted ages in the cluster and the field, finding that massive galaxies form earlier, and quicker than low mass galaxies, and that cluster galaxies are older than the field.

The discrepancy in both of these cases with the findings in the local Universe lead to the interpretation that a different quenching mode must be in play early in cluster formation. With the information added from studying transition populations, we see that the green valley population fraction is consistent with the field, with no excess in the cluster, and that the quenching rate of the green valley is consistent with the past average, indicating no significant difference in the quenching mechanism over time.

Though all three transition populations are distinct in the way they have been selected, they are consistent with a scenario where fast quenching is essential in cluster evolution. The analysis of the green valley shows that transformations as a fraction of the star-forming population within the cluster are happening at a rate of 0.08/Gyr, and coupled with the excess of BQGs and PSBs in the cluster indicate that most of this transition is happening via fast-quenching, acting over short timescales. Even at the early times considered in this work, it appears that the environmental processes that are quenching star formation in cluster galaxies are already taking place. The constant rate of this environmental quenching indicates that it is more likely due to more universal processes like

strangulation, as opposed to those such as ram-pressure stripping which are more prevalent in massive, evolved systems. Taking into account merging where this simple model does not, and using more sophisticated stellar modeling would be beneficial for future work. Studying the green valley, though a complete sample of transitioning galaxies, contains few galaxies (10%) that are being environmentally quenched. Further work would benefit from using a different definition of transitioning galaxies to obtain a more pure sample of this population.

References

Arnouts S., et al., 2007, A&A, 476, 137

Bahé Y. M., et al., 2017, MNRAS, 470, 4186

Baldry I. K., Balogh M. L., Bower R., Glazebrook K., Nichol R. C., Bamford S. P., Budavari T., 2006, Monthly Notices of the Royal Astronomical Society, 373, 469

Balogh M. L., Schade D., Morris S. L., Yee H. K., Carlberg R. G., Ellingson E., 1998, The Astrophysical Journal Letters, 504, L75

Balogh M. L., Morris S. L., Yee H. K. C., Carlberg R. G., Ellingson E., 1999, ApJ, 527, 54

Balogh M. L., et al., 2016, MNRAS, 456, 4364

Balogh M. L., et al., 2017, MNRAS, 470, 4168

Balogh M. L., et al., 2021, MNRAS, 500, 358

Behroozi P. S., Wechsler R. H., Conroy C., 2013, ApJ, 770, 57

Behroozi P., et al., 2019, Unknown Journal

Belli S., Newman A. B., Ellis R. S., 2019, ApJ, 874, 17

Bower R., Benson A., Malbon R., Helly J., Frenk C., Baugh C., Cole S., Lacey C. G., 2006, Monthly Notices of the Royal Astronomical Society, 370, 645

Brodwin M., et al., 2010, ApJ, 721, 90

Carnall A. C., et al., 2019, MNRAS, 490, 417

Chan J. C. C., et al., 2019, ApJ, 880, 119

Coenda V., Martínez H. J., Muriel H., 2018, Monthly Notices of the Royal Astronomical Society, 473, 5617

Cole S., 1991, The Astrophysical Journal, 367, 45

Cole S., Lacey C. G., Baugh C. M., Frenk C. S., 2000, Monthly Notices of the Royal Astronomical Society, 319, 168

Cole S., et al., 2005, Monthly Notices of the Royal Astronomical Society, 362, 505

Couch W. J., Sharples R. M., 1987, MNRAS, 229, 423

Demarco R., et al., 2010, ApJ, 711, 1185

Dressler A., 1980, The Astrophysical Journal, 236, 351

Dressler A., Gunn J. E., 1983, ApJ, 270, 7

Dressler A., Gunn J. E., 1992, ApJS, 78, 1

Drory N., et al., 2009, ApJ, 707, 1595

Faber S. M., et al., 2007, ApJ, 665, 265

Foley R. J., et al., 2011, ApJ, 731, 86

Gómez P. L., et al., 2003, ApJ, 584, 210

Gunn J. E., Gott III J. R., 1972, The Astrophysical Journal, 176, 1

Hogg D. W., Masjedi M., Berlind A. A., Blanton M. R., Quintero A. D., Brinkmann J., 2006, ApJ, 650, 763

Kauffmann G., White S. D., Heckman T. M., Ménard B., Brinchmann J., Charlot S., Tremonti C., Brinkmann J., 2004, Monthly Notices of the Royal Astronomical Society, 353, 713

Kriek M., Van Dokkum P. G., Labbé I., Franx M., Illingworth G. D., Marchesini D., Quadri R. F., 2009, The Astrophysical Journal, 700, 221

Leja J., Tacchella S., Conroy C., 2019, ApJ, 880, L9

Lewis I., et al., 2002, MNRAS, 334, 673

McGee S. L., Bower R. G., Balogh M. L., 2014, MNRAS, 442, L105

McLeod D., McLure R., Dunlop J., Cullen F., Carnall A., Duncan K., 2021, Monthly Notices of the Royal Astronomical Society, 503, 4413

Mendez A. J., Coil A. L., Lotz J., Salim S., Moustakas J., Simard L., 2011, ApJ, 736, 110

Mok A., et al., 2013, MNRAS, 431, 1090

Mok A., et al., 2014, MNRAS, 438, 3070

Moore B., Katz N., Lake G., Dressler A., Oemler A., 1996, nature, 379, 613

Moster B. P., Somerville R. S., Maulbetsch C., Van Den Bosch F. C., Maccio A. V., Naab T., Oser L., 2010, The Astrophysical Journal, 710, 903

Moutard T., et al., 2016, A&A, 590, A103

Moutard T., Sawicki M., Arnouts S., Golob A., Malavasi N., Adami C., Coupon J., Ilbert O., 2018, MNRAS, 479, 2147

Muzzin A., et al., 2009, ApJ, 698, 1934

Muzzin A., et al., 2012, ApJ, 746, 188

Muzzin A., et al., 2013a, The Astrophysical Journal, 777, 18

Muzzin A., et al., 2013b, ApJ, 777, 18

Muzzin A., et al., 2014, ApJ, 796, 65

Noeske K. G., et al., 2007, ApJ, 660, L43

Old L. J., et al., 2020, MNRAS, 493, 5987

Paccagnella A., Vulcani B., Poggianti B. M., Moretti A., Fritz J., Gullieuszik M., Fasano G., 2019, MNRAS, 482, 881

Patel S. G., Holden B. P., Kelson D. D., Illingworth G. D., Franx M., 2009, ApJ, 705, L67

Pattarakijwanich P., Strauss M. A., Ho S., Ross N. P., 2016, ApJ, 833, 19

Peacock J. A., et al., 2001, Nature, 410, 169

Peng Y.-j., et al., 2010, ApJ, 721, 193

Poggianti B. M., Smail I., Dressler A., Couch W. J., Barger A. J., Butcher H., Ellis R. S., Oemler Augustus J., 1999, ApJ, 518, 576

Poggianti B. M., et al., 2006, ApJ, 642, 188

Poggianti B. M., et al., 2009, ApJ, 693, 112

Salim S., 2014, Serbian Astronomical Journal, 189, 1

Salim S., et al., 2007, ApJS, 173, 267

Santini P., et al., 2012, A&A, 538, A33

Schawinski K., et al., 2014, MNRAS, 440, 889

Schiminovich D., et al., 2007, ApJS, 173, 315

Smethurst R. J., et al., 2015, MNRAS, 450, 435

Socolovsky M., Almaini O., Hatch N. A., Wild V., Maltby D. T., Hartley W. G., Simpson C., 2018, MNRAS, 476, 1242

Stalder B., et al., 2013, ApJ, 763, 93

Strateva I., et al., 2001, AJ, 122, 1861

Suess K. A., Kriek M., Price S. H., Barro G., 2020, ApJ, 899, L26

Takamiya M., Kron R. G., Kron G. E., 1995, The Astronomical Journal, 110, 1083

Tran K.-V. H., Franx M., Illingworth G. D., van Dokkum P., Kelson D. D., Magee D., 2004, ApJ, 609, 683

Vulcani B., Poggianti B. M., Fritz J., Fasano G., Moretti A., Calvi R., Paccagnella A., 2015, ApJ, 798, 52

Webb K., et al., 2020, MNRAS, 498, 5317

Weinmann S. M., Van Den Bosch F. C., Yang X., Mo H., 2006, Monthly Notices of the Royal Astronomical Society, 366, 2

Wetzel A. R., Tinker J. L., Conroy C., 2012, MNRAS, 424, 232

Whitaker K. E., van Dokkum P. G., Brammer G., Franx M., 2012, ApJ, 754, L29

White S. D., Frenk C. S., 1991, The Astrophysical Journal, 379, 52

Wild V., Almaini O., Dunlop J., Simpson C., Rowlands K., Bowler R., Maltby D., McLure R., 2016, MNRAS, 463, 832

Wild V., et al., 2020, MNRAS, 494, 529

Williams R. J., Quadri R. F., Franx M., van Dokkum P., Labbé I., 2009, ApJ, 691, 1879

Wilson G., et al., 2009, ApJ, 698, 1943

Yan R., et al., 2009, MNRAS, 398, 735

Zabludoff A. I., Zaritsky D., Lin H., Tucker D., Hashimoto Y., Shectman S. A., Oemler A., Kirshner R. P., 1996, ApJ, 466, 104

van den Bosch F. C., Aquino D., Yang X., Mo H. J., Pasquali A., McIntosh D. H., Weinmann S. M., Kang X., 2008, MNRAS, 387, 79

van der Burg R. F. J., et al., 2013, A&A, 557, A15

van der Burg R. F. J., et al., 2020, A&A, 638, A112

APPENDICES

Appendix A

Cluster Core Radial Cut

We followed the same analysis mentioned throughout this paper considering a smaller radial cut, within 0.5 Mpc of the cluster center, and find consistent results, which rules out that there might be a radial trend that is being missed due to coarse binning.

We see from Figure 3.1 that the cluster population composition differs from the field most strongly within the inner 0.5 Mpc. We therefore also consider the SMFs limited to that volume, shown in Figure A.2. Qualitatively the picture is unchanged - in particular the quiescent galaxies have the flat faint end slope characteristic of the quiescent population, significantly different from that of the star-forming galaxies.

Table A.1: Schechter mass function fits, for each of the galaxy populations for the 0.5 Mpc cluster cut.

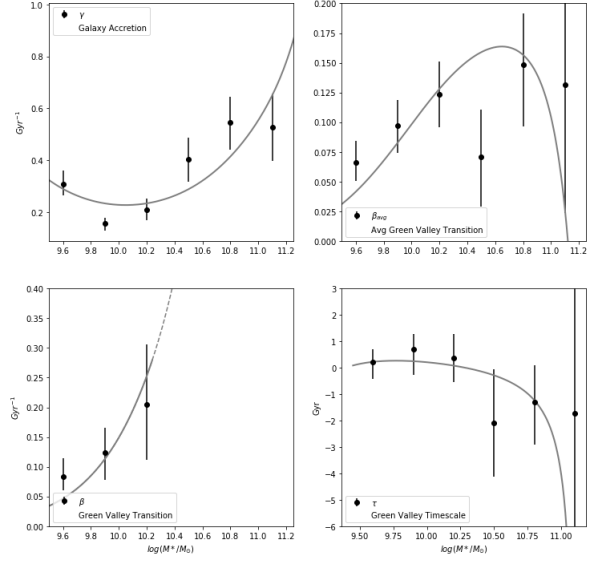|		χ^2	$log_{10}(M^*/M_\odot)$	α	ϕ^*
	SF	34.37	11.49	-1.72	6.49 $\times 10^{-12}$
r <0.5 Mpc	Qui	8.33	10.87	-0.35	1.06 $\times 10^{-9}$
	GV	1.82	10.90	-0.72	1.32 $\times 10^{-10}$
	Total	45.29	11.10	-0.93	5.39 $\times 10^{-10}$

Figure A.1: The transition parameters as a function of mass as described in Equations 3.5, 3.11, 3.14 and 3.16. Analagous to Figure 3.6, but for a cluster cut within 0.5 Mpc of the center.
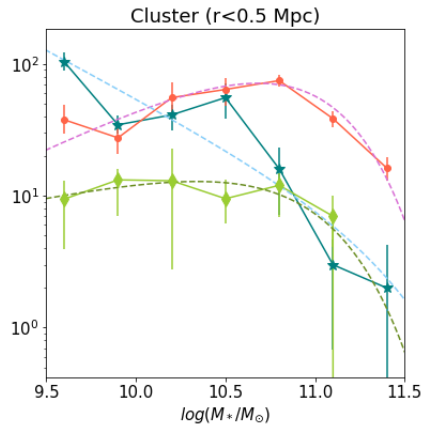

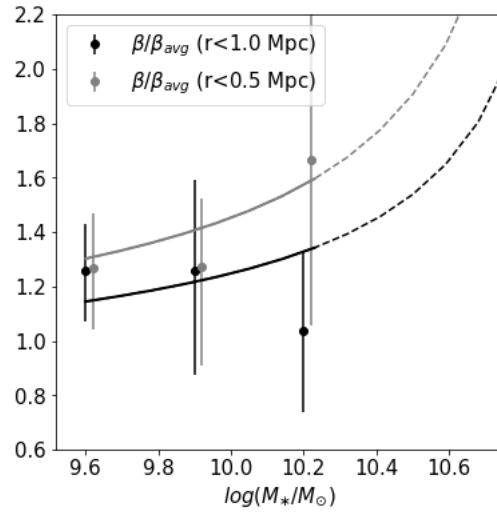Figure A.2: The mass functions for each of the populations, along with their Schechter fits.

Figure A.3: The ratio of the current to past average environmental quenching rate, $\beta(T)/\beta_{avg}$ for both radial cuts for comparison. The points represent the measurements and the lines are derived from the Schechter function fit parameters.

Appendix B

Quenched Fraction Excess

The Quenched Fraction Excess is defined as

$$\text{QFE} = \frac{f_{\text{NSF}}^{C} - f_{\text{NSF}}^{F}}{1 - f_{\text{NSF}}^{F}}, \tag{B.1}$$

where f_{NSF}^{C} and f_{NSF}^{F} are the fractions of non-star forming galaxies in the cluster and field respectively. The non-star forming population, in the present paper, is made up of both Quiescent and green valley galaxies, so so $f_{\text{NSF}}^{i} = 1 - \phi_{S}^{i}/\phi^{i}$, using our notation for the SMF from § 3.3:

$$\text{QFE} = \frac{\left(\phi^{C} - \phi_{S}^{C}\right)/\phi^{C} - \left(\phi^{F} - \phi_{S}^{F}\right)/\phi^{F}}{\phi_{S}^{F}/\phi^{F}}. \tag{B.2}$$

Simplifying, this yields

$$\text{QFE} = \left(\frac{\phi_{S}^{F}}{\phi^{F}} - \frac{\phi_{S}^{C}}{\phi^{C}}\right)\frac{\phi^{F}}{\phi_{S}^{F}} = 1 - \frac{\phi_{S}^{F}}{\phi^{F}}\frac{\phi_{S}^{C}}{\phi_{S}^{F}} = T\beta_{avg} \tag{B.3}$$

where the last equality follows from Equation 3.11.
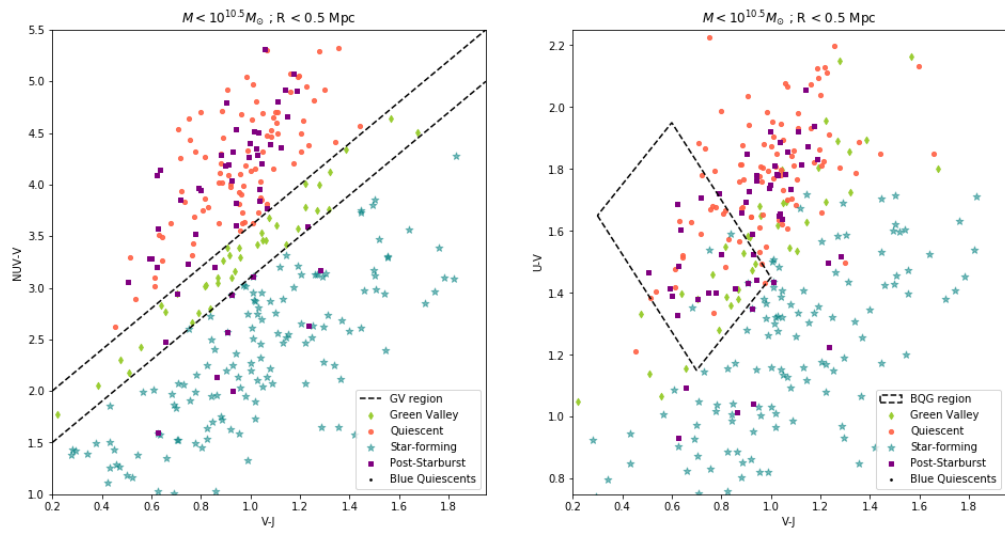
Appendix C

Additional figures

Figure C.1: Analogous Figure 4.6, but with inner radial cut and for low masses.
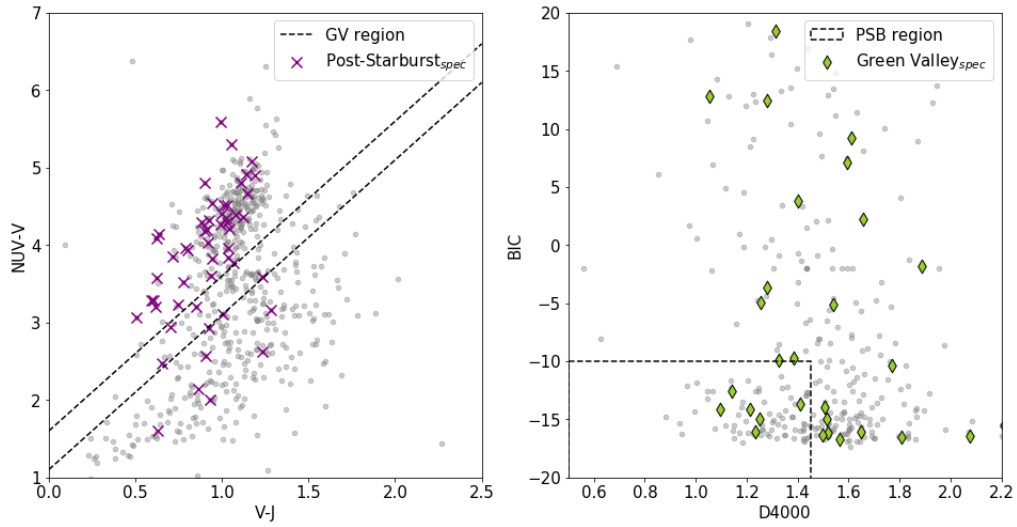
Figure C.2: The spectroscopic post-starburst galaxies are defined using spectroscopy, limited to those that have $D4000 < 1.45$ and $BIC < -10$, shown as the region in the box in the right panel. The galaxies found to be spectroscopically post-starburst are shown overlaid (in purple) in NUV-V V-J space in the left panel to compare their overlap with the photometric green valley. To compare the green valley with the post-starbursts, we limit the green valley points (green) over-plotted on the right panel to those with spectroscopy, giving us a depiction of the overlap with the BIC and D4000 defined post-starbursts.